Water Science & Technology

IWA PUBLISHING

Water Science & Technology Vol 85 No 10, 3036 doi: 10.2166/wst.2022.092

Preparation, characterization, and application of modified magnetic biochar for the removal of benzotriazole: process optimization, isotherm and kinetic studies, and adsorbent regeneration

Maryam Hasanzadeh[a], Yaser Soltaninejad[a], Shirin Esmaeili[a] and Ali Akbar Babaei[a,b,*]

[a] Department of Environmental Health Engineering, School of Public Health, Ahvaz Jundishapur University of Medical Sciences, Ahvaz, Iran
[b] Environmental Technologies Research Center, Ahvaz Jundishapur University of Medical Sciences, Ahvaz, Iran
*Corresponding author. E-mail: babaei-a@ajums.ac.ir

ABSTRACT

The adsorption of benzotriazole (BTA) by chemically modified magnetic biochar (MMBC) as a cheap and abundant biosorbent was investigated and optimized using response surface methodology (RSM). Initially, the MMBC composite was synthesized and characterized by scanning electron microscopy (SEM) energy dispersive X-ray spectroscopy (EDX), Fourier transform infrared spectroscopy (FTIR), Raman spectroscopy, and Brunauer–Emmett–Teller (BET) techniques. The characterization results confirmed the existence of Fe_3O_4 in the composite structure, which had uniformly dispersed over biochar (BC) with porous texture. Moreover, the presence of Zn and Cl elements in EDX analysis indicated that the magnetic biochar (MBC) had been modified successfully. The effects of chemical modification methods on the adsorption capacity of magnetic biochar were investigated. Maximum BTA removal efficiency was demonstrated by MMBC, modifying using $ZnCl_2$ (>99%). Optimization was carried out based on reaction time, BTA concentration and the concentration of adsorbent. Optimum experimental conditions for the removal of BTA from aqueous solutions were found to be 35 min of reaction time, 0.55 g/L of adsorbent, and 50 mg/L of initial BTA concentration. At these optimal conditions, the predicted BTA adsorption efficiency was 92.6%. The adsorption process followed the Avrami fractional-order reaction kinetic and the Langmuir adsorption isotherm with the maximum adsorption capacity of 563.1 mg/g. The values of thermodynamic parameters demonstrated that the adsorption of BTA on $ZnCl_2$-MBC is endothermic and spontaneous. Under optimum usage of MMBC, the adsorptive removal efficiency of BTA non-significantly decreased from 99.2 to 93.9% after the 5th cycle. Thus, MMBC can be recommended as an environmentally friendly and cost-effective adsorbent to remove micropollutants from water.

Key words: benzotriazole, central composite design, modified magnetic biochar, response surface methodology, reusability

HIGHLIGHTS

- Among all chemical modification methods, $ZnCl_2$ showed the maximum adsorptive removal of BTA (>99%).
- At optimum experimental conditions for the removal of BTA, adsorption efficiency was calculated 92.6%.
- The adsorption process followed the Avrami fractional-order reaction kinetic and the Langmuir adsorption isotherm with the maximum adsorption capacity of 563.1 mg/g.

GRAPHICAL ABSTRACT

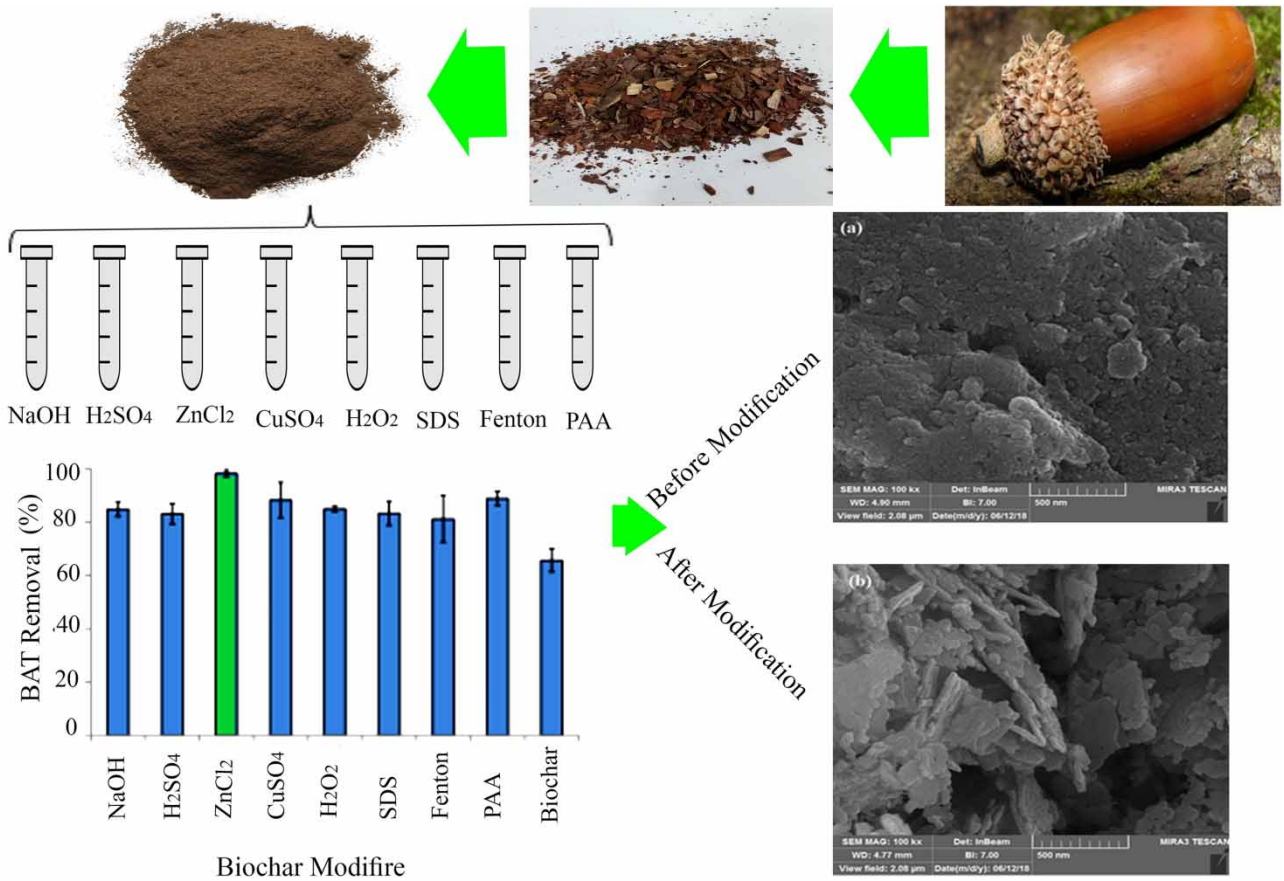

1. INTRODUCTION

Benzotriazole (BTAs) is a polar conditioning chemical (CCs) that possesses a low log K_{ow} value of 1.23, which it presents in sediments and soil, surface water, and groundwater. BTA is commonly applied as a corrosion inhibitor in engine coolants, anti-freeze liquids, detergent additives, aircraft de-icing and anti-icing substances, hydraulic fluids, and a stabilizer for bronze commodities (Janna *et al.* 2011; Li *et al.* 2012; Mezzi *et al.* 2012; Grillo *et al.* 2013). However, it is classified as an emerging pollutant, and it is known to be toxic to vertebrates (LC_{50} of 102 mg/L for water fleas *Ceriodaphnia dubia*); also, it has adverse effects such as anti-estrogenic and carcinogenesis effects (Harris *et al.* 2007; Pritchard *et al.* 2018; Richardson & Ternes 2018). BTA and its derivatives are regularly discharged in municipal/industry wastewater, resulting in high natural surface/groundwaters (Xu *et al.* 2014). They are often contaminated with BTA due to their high solubility in water, limited removal efficiency, and extensive applications (Giger *et al.* 2006). Nonetheless, limited information is available about the possible release of BTA into the environment, particularly in water resources (Richardson & Ternes 2018).

BTA removal is limited and challenging in wastewater treatment plants due to its non-biodegradability and resistance to disintegration (Rhodes-Dicker & Passeport 2019). Therefore, diverse methods including oxidation processes (Mawhinney *et al.* 2012), membrane bioreactors (Weiss & Reemtsma 2008), photoelectrocatalytic degradation (Ding *et al.* 2010), and adsorption (Xu *et al.* 2014) have been employed for the removal of BTA from aqueous solutions. However, the application of these technologies is limited by some factors such as low efficiency, detrimental byproducts, and high operation costs (Bernal-Martínez *et al.* 2013).

Among different BTA removal systems, adsorption is an efficient and low-cost process. To date, a number of adsorbents, such as carbonaceous materials (Bonvin *et al.* 2016), zeolites (Wang *et al.* 2017), and metal oxides have been used aiming at BTA adsorption from aqueous solutions (Sarker *et al.* 2017); however one of the most important aspects related to water and

wastewater treatment is finding cost-effective adsorbents. Recently, the utilization of cheap carbon adsorbents (Biochar) from waste products and low-cost compounds has been prevalent (Dai *et al.* 2019). Biochar is a carbon-rich solid characterized by porous structure, large surface functional groups, and mineral components, making it a proper adsorbent for removing pollutants from aqueous solutions (Dai *et al.* 2019). Nonetheless, bare biochar has a low adsorptive capacity to adsorb contaminants in water and sewage treatment. Moreover, powdered adsorbents are tenacious to separate from effluents after adsorption. Separation via filtration and centrifugation methods may not completely isolate the adsorbent from the effluent; therefore, magnetized biochar has been considered a suitable solution to tackle this challenging problem (Khan *et al.* 2020). On the other hand, adsorption processes are mainly affected by various operational factors, including contact time, adsorbent dosage, initial concentration of contaminant, etc.; it is beneficial to utilize appropriate experimental methods. These mathematical and statistical methods can create a systematic path that permits the final goal (removal efficiency) to be based on influential parameters, which are the most dominant in the response factor, by the at least possible number of experiments for decline process expenditure and required time to developing of process installation (Haghighi *et al.* 2019). Response surface methodology (RSM) is one of the effective multivariate experimental design methods. This approach comprises several mathematical and statistical techniques that are employed to develop, improve and optimize various processes and analyze the relative significance of each operational condition even in the presence of a complex network of interactions (Najafpoor *et al.* 2019).

Several studies have employed modified magnetic biochar (MMBC) for the adsorption of a wide range of pollutants such as nitrate and phosphate (Yin *et al.* 2018), tetracycline (Zhou *et al.* 2019), methylene blue (Liu *et al.* 2019), 2,4-dichlorophynoxyacetic acid (Zhu *et al.* 2018), cadmium adsorption (Cui *et al.* 2019), and Remazol Brilliant Orange (Gokulan *et al.* 2019). However, to the best of our knowledge, few studies have focused on optimizing the BTA adsorption process using MMBC, modified with different modifiers and their efficiency compared with each other and its regeneration. In the present research, a porous MBC adsorbent was synthesized and characterized using various techniques (Najafpoor *et al.* 2019). The composite was modified with multiple chemicals, and then the best-modified composite was chosen for main experiments. The RSM based on central composite design (CCD) was adopted for modeling, analyzing, and optimizing the BTA removal process by MMBC as a function of three independent variables (reaction time (min), adsorbent dosage (g/L), and initial BTA concentration (mg/L)). The importance of each independent variable on the variation of the output response (BTA removal efficiency (%)) was also determined. Moreover, isotherm, kinetic, thermodynamic studies were conducted. Finally, MMBC adsorbent reusability study via different regenerators was investigated in detail.

2. MATERIALS AND METHODS

2.1. Chemicals

BTA with the formula $C_6H_5N_3$ (Table 1), sodium hydroxide (NaOH), condensed sulfuric acid H_2SO_4, $ZnCl_2$, sodium dodecyl sulfate (SDS), and per acetic acid (PAA) were purchased from Merck Co. (Germany). All chemicals were of analytical grade. Ultrapure water was used for preparing solutions.

Table 1 | The characteristics of BTA

Item	Description
Formula	$C_6H_5N_3$
Synonym	1,2,3-Benzotriazole & 1H-Benzotriazole
Structure	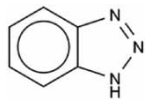
Molecular weight	119.12
pH	6.0–7.0 at 100 g/l at 20 °C – (aqueous suspension)
Partition coefficient: n-octanol/water	log Pow: 1.44
LD50 Oral – Rat	500 mg/kg
LD50 Dermal – Rat	>1,000 mg/kg
[a]pK_a	1.6, 8.6

[a]pK_{a1} and pK_{a2} for protonated and neutral BTA are 1.6 and 8.6, respectively.

2.2. Preparation and modification of adsorbents

For biochar synthesis, Oakwood residues were rinsed, dried at 105 °C for 24 hours, crushed, and sieved (5-mm) to remove big lumps; then, it was stored in a sealed container an incubator for the experiment. Next, the biomass powder was heated from room temperature to 700 °C with a heating rate of 5 °C/min. The pyrolysis process was performed using a tube furnace with continuous nitrogen gas purging at 30 ml/min and the heating rate was constant at 15 °C/min. For promoting the functional group on biochar surface, the achieved biochar (2.5 g) was reacted with $ZnCl_2$ solution (the weight ratio of 2:1) at 100 °C for 2 h. Then, the reaction mixture was added to deionized water (100 mL), and precipitates were separated by filtration. The excess $ZnCl_2$ was washed by applying dilute hydrogen chloride. Subsequently, carbon was repeatedly washed to eliminate excess $ZnCl_2$, and was then dried at 60 °C for 12 h. Modification of BC with other chemicals obeys such a mentioned process and weight ratio.

An aqueous solution of NH_3 (15 mL, 25%) was added dropwise with powerful stirring under nitrogen flow for 1.5 h to a mixture of MBC (2.0 g), $FeCl_3.6H_2O$ (2.7 g), $FeCl_2.4H_2O$ (2.5 g), and deionized water (60 mL). Next, the black solid was gathered by an external magnet, washed with distilled water (three times), and dried at 60 °C for 5 h. The obtained $ZnCl_2$/MBC was utilized for the BTA adsorption process.

2.3. Batch adsorption studies

The adsorption experiments for BTA removal were conducted in a batch system at room temperature. The 0.1M NaOH and 0.1M H_2SO_4 solutions were applied to adjust the pH of BTA solutions. pH: 2–10, adsorbent size <105–1,000 μm, $ZnCl_2$ concentration: 5–200 g/L, retention time: 0–60 min, adsorbent dosage: 0.1–1 g/L, and BTA concentration: 10–90 mg/L were used as variables in this study. The batch experiments were performed in a 500 mL glass vessel, with 100 mL of BTA being used at different initial concentrations (10, 30, 50, 70 and 90 mg/L). Samples were collected at the determined times and immediately filtered by 0.45 μm cellulose acetate membranes to separate the adsorbent from the supernatant. The concentrations of the remaining BTA were measured by UV spectrometric (UV-1800, Shimadzu, Japan). The UV absorbance 259 nm was applied to calculate the BTA concentration. The removal efficiency of BTA (% R) and the adsorption capacity of the adsorbent were calculated using Equations (1) and (2), respectively:

$$R\,(\%) = \frac{C_o - C_e}{C_e} \times 100 \tag{1}$$

$$q_e = \frac{(C_o - C_e)V}{m} \tag{2}$$

where C_o and C_e are the initial and residual BTA concentrations (mg/L), respectively, q_e is the BTA adsorption capacity (mg/g), V is the volume of BTA solution (L), and m is the mass of the adsorbent (g). All experiments were performed in triplicate, and the average data were reported.

2.4. Response surface methodology

2.4.1. Experimental design

The influence of the selected variables (reaction time, adsorbent concentration, and initial BTA concentration) on the adsorptive removal of BTA was evaluated. To this end, a CCD with three experimental factors and three levels was employed to reach the optimum experimental conditions for BTA removal and monitor the impact of each parameter and the parameters' interaction effects. In this pattern, the total number of experiments consisting of 18, 6, and 8 experiments in central, axial, and factorial points, respectively, were determined using Equation (3):

$$N = 2^k + 2k + C_o \tag{3}$$

where N denotes the total number of experiments, k represents the number of experimental variables, and 2^k, $2\,k$, and C_o are the factorial, axial, and central points, respectively.

The second-order polynomial model for the prediction of the relationship between experimental and predicted values is expressed as follows (Equation (4)):

$$y = b_0 + \sum b_i x_i + \sum b_{ii} x_i^2 + \sum b_{ij} x_i + \varepsilon \tag{4}$$

In which y is the response, b_o is the constant term, b_i is the coefficient of the linear effect, b_{ij} represents the coefficient of the interaction effects of variables, and ε is the residual term.

For enhancing the simplicity of statistical calculations, Equation (5) was employed to code each variable level as x_i (Sarangi *et al.* 2018).

$$x_i = \frac{X_i - X_o}{\Delta X_i} \tag{5}$$

where X_o demonstrates the value of X_i at the center point, and ΔX_i is the step change. Table 2 represents the ranges and actual values of the applied parameters. Based on the preliminary experiments, the pH of 7.0 was considered the optimum pH of the solution in all experiments.

2.4.2. Estimation of the applied model

For evaluation of the second-order polynomial model reliability, normal plots, residual examination, and ANOVA were performed. In addition, adjusted *R*-square and *F*-test were applied to check the quality and statistical significance of the model, respectively. The *F*-test and Student's *T*-test were used to test the importance of the model at a 95% confidence level. Furthermore, the residuals (the differences between experimental and predicted values) were analyzed through residual and normal probability plots to examine the constant variance of errors; also normal distribution was assessed to detect possible systematic departures from the assumption.

Pareto calculations were performed to examine the effect of each parameter and their interaction effects on the response parameters based on Equation (6) (Abdessalem *et al.* 2008):

$$P_i = \left(\frac{b_i^w}{\sum b_i^w}\right) \times 100 \quad i \neq 0 \tag{6}$$

This study used the Design-Expert (version 8.0.0) software package to design experiments, model-fitting, and data analysis.

2.5. Adsorption isotherm and kinetic models

Concerning the adsorptive remediation of water and wastewater containing contaminants, it is essential to know the removal rate for the design and the quantitative evaluation of the adsorbent. In addition, kinetics describes the adsorbate uptake rate, which controls the residence time of the adsorbate uptake at the adsorbent–solution interface. Therefore, it is vital for prediction of the BTA uptake removal rate from aqueous solutions in order to design an appropriate adsorption unit.

The BTA adsorption data were fitted to the non-linear kinetic and isotherm models using MATLAB® 7.11.0 (R2015b), with subsequent interactions calculated by the Levenberg–Marquardt algorithm. Since the unwanted falsification of error distribution occurs due to data transformation to a linear form, the non-linear method is superior to the linear one in determining the parameters of the isotherm and kinetic models. In this study, five widely used adsorption isotherm models (Langmuir, Freundlich, Redlich–Peterson, Temkin, and Liu) and five general adsorption kinetic models (pseudo-first-order equation of Lagergren, pseudo-second-order equation of Ho, Elovich, Avrami fractional order, and the intraparticle diffusion model) were used to describe the adsorption equilibrium and the adsorption kinetics of BTA onto MMBC, respectively (Vilardi *et al.* 2018; Zhang *et al.* 2018; Jeon 2019; Rezakazemi & Shirazian 2019; Syafiuddin *et al.* 2019). All these mathematical isotherms and kinetic models are summarized in Supplementary Table 1.

Table 2 | Coded and actual values of the experimental variables

	Limits and levels				
Independent variables	**−2**	**−1**	**0**	**+1**	**+2**
Contact time (min) (X_T)	5	20	35	50	65
Adsorbent dose (mg/L) (X_D)	0.05	0.3	0.55	0.80	1.05
Initial BTA concentration (mg/L) (X_{Co})	10	30	50	70	90

It is essential to evaluate their validity to select the most suitable kinetic and isotherm model. Here, the validity of the kinetic and isotherm models at different temperatures (283, 298, and 313 K) was assessed by criteria such as the determination coefficient (R^2), the adjusted determination coefficient (R^2adj), the sum squared error (SSE), and the root mean square error (RMSE) (Rangabhashiyam *et al.* 2014; Suganya 2019). These criteria describe the goodness of fit between the experimental and predicted data. The best model was chosen based on the lowest RMSE, SSE, and R^2adj and R^2 as close as possible to 1. R^2, R^2adj, SSE, and RMSE were calculated according to Supplementary Table 2.

2.6. Reusability study of MMBC

To evaluate the possibility of MMBC regeneration and reuse, methanol, as a desorbing solution, was utilized to extract the BTA adsorbed on MMBC. The reusability of the adsorbents was determined using five adsorption–regeneration cycles. A sample of 1.0 g of MMBC was shaken with 1 L solution of 50 mg/L BTA for 1 h at 25 ± 1 °C and pH = 7.0. The BTA-loaded MMBC was magnetically collected, washed, and shaken at 200 rpm for 24 h with 10 mL of desorbing solutions methanol at 25 ± 1 °C. After desorption, regenerated adsorbents were dried in an oven at 80.0 °C for 100 min and used for the next adsorption-regeneration cycle.

3. RESULTS AND DISCUSSION

3.1. MMBC characterization

Table 3 represents some physicochemical characteristics of the adsorbent. The elemental analysis demonstrated that C (49%) is the dominant element in the composite structure; also, the presence of O (18.43%) and Fe (9.42%) indicated that the magnetization agent had been loaded correctly on biochar. Moreover, results confirmed the existence of Zn (9.07%) and Cl (13.85%) as a modifier in the MMBC structure. The specific surface area of MMBC (383.5 g/m^2) was determined by BET analysis; this high value can be attributed to the increased surface area of loaded iron oxide nanoparticle and modification by $ZnCl_2$, which is beneficial to the increasing adsorption capacity of biochar in BTA adsorption; whereas, the specific surface areas for BC and MBC were 210 and 297 g/m^2, respectively. Moreover, the morphology of the samples was examined with an FEI Quanta 400 FEG scanning electron microscope (SEM), and the SEM image of MMBC is illustrated in Figure 1(a) and 1(b). Based on Figure 1(a), it is evident that the BC surface was relatively smooth and had a porous structure, without significant development on its surface. However, based on the SEM images (Figure 1(b)), the produced modified biochar had a relatively rough, much more porous structure than BC.

Table 3 | The physicochemical characteristics of MMBC

Parameters	Values
Moisture content (%)	1.65 ± 0.4
Water-soluble compounds (%)	1.0 ± 0.2
Insoluble compounds (%)	97.35 ± 0.4
Volatile fraction (%)	67.7 ± 1.4
Ash content (%)	32.3 ± 1.3
Elemental analysis (%)	
C	49.2
O	18.43
Zn	9.07
Fe	9.42
Cl	13.85
pH_{ZPC}	5.0 ± 0.2
Bulk density (kg/m^3)	858
Particle size (μm)	<105
BET surface area (m^2/g)	383.5

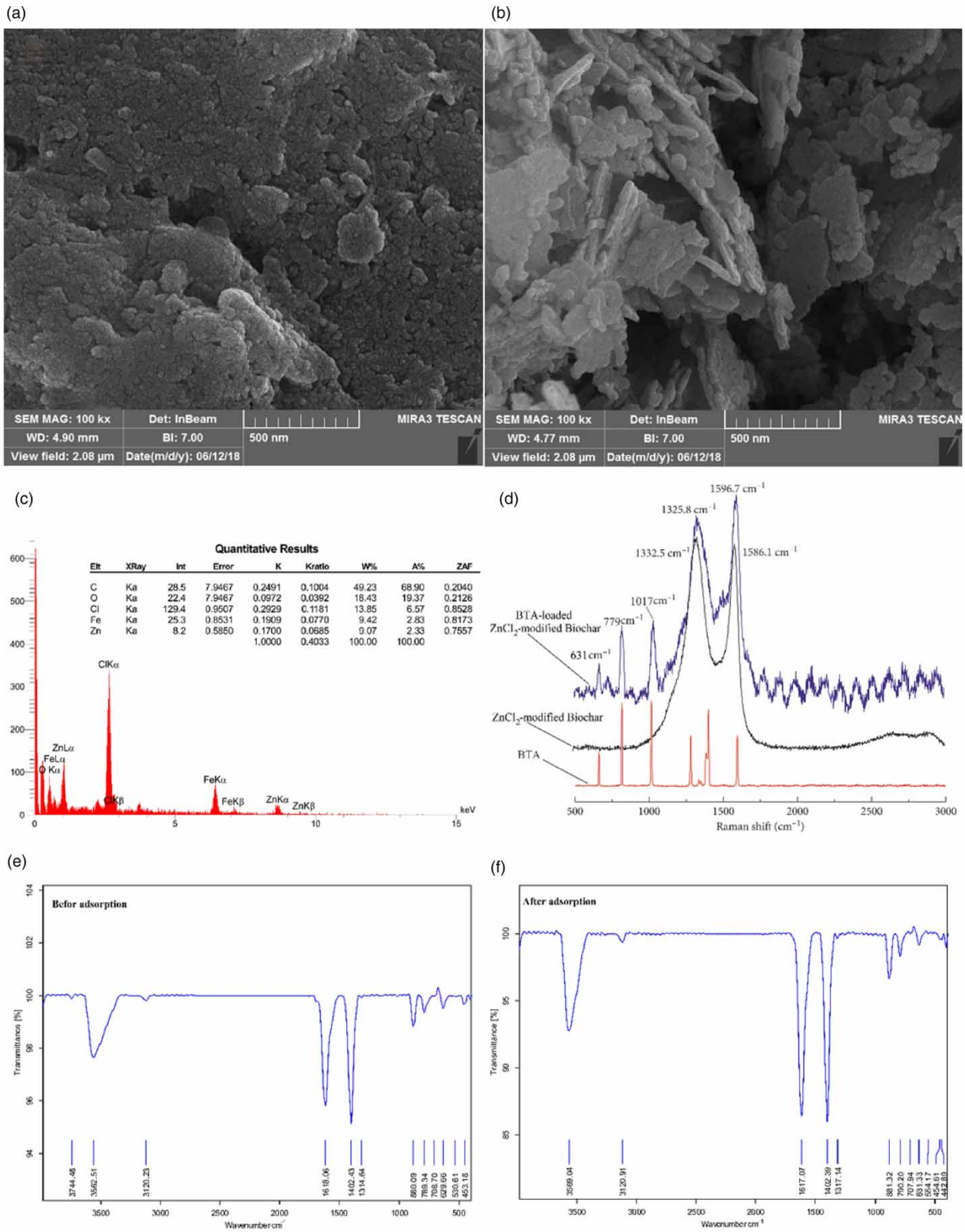

Figure 1 | SEM images of adsorbent: (a) before modification (b) after modification, (c) EDX spectra of adsorbent (d) Raman spectroscopy of adsorbent, FTIR of adsorbent: (e) before reaction with BTA, (f) after reaction with BTA.

Moreover, Fe_3O_4 nanoparticles tended to aggregate on the BC surface, and a vigorous aggregation is evident after magnetization. This phenomenon can create a rough and uneven surface followed by increased adsorption sites for BTA adsorption. It is worth noting that the white parts in the SEM may be attributed to the zinc salt residues. It seems that the cavities on the surface of biochar resulted from the $ZnCl_2$ evaporation during carbonization, leaving the space previously occupied by zinc chloride. The pore-forming effect of $ZnCl_2$ decomposition during heat treatment could promote the organic compound breakage in the precursor of BC (Oakwood residues) residues and gradually recombine the solid matrix to form an extended porous structure, which could accelerate the reaction rate, raise the surface area, and provide more active sites for the adsorption of BTA (Yan *et al.* 2020). Energy dispersive X-ray (EDX) analysis, including spectrum and elemental composition (Figure 3), illustrating BC/Fe_3O_4 nanocomposite contains peaks responding to the C, Fe, O, Cl, and Zn atoms. The peaks of Fe (9.42%) and O (18.43%) are related to Fe_3O_4, while the C (49.23%) atom is associated with BC. In addition, Cl (13.85%) and Zn (9.07%) confirmed the modification of MBC by $ZnCl_2$.

Raman spectroscopy (PerkinElmer Raman Station 400F dispersive Raman micro-spectrometer with a CCD detector) was applied to investigate the chemical functionality and mineralogy of biochar. Raman was conducted at the wavelength of 500–300 cm^{-1} (Figure 1(d)). The highest peak was observed at 1,596 cm^{-1} and 1,325 cm^{-1}. The peaks at 799 and 1,017 cm^{-1} were assigned as a D-band, as well as the peaks at 1,332 cm^{-1} and 1,586 cm^{-1} are related to G-band peaks in the Raman spectra. Different biomass-derived biochar has typical characters associated with the structural disordered aromatic ring in sp^2 carbon atoms or sample defective graphite structure (D-band), in contrast, G-band presents completeness of the degree of sp^2 carbon atoms with less defective graphene structures (Liu *et al.* 2021). Additionally, Fourier transform infrared (FTIR) spectra of the MMBC before and after reaction with BTA are illustrated in Figure 1(e) and 1(f). The FTIR spectra of biochar were recorded in 4,000–500 cm^{-1}. The peak at 3,569 cm^{-1} is a firm indicator of the OH phenol functional group onto the surfaces of the adsorbent. The two sharp peaks at 1,402 cm^{-1} and 1,617 cm^{-1} are related to the amine functional group and the symmetric bending of CH_3, respectively. Based on Figure 1, among the surface functional groups, –OH groups, secondary amine group, C = O stretching of ether group, aliphatic C–H group, C–N stretch of aliphatic amines, and symmetric bending of CH_3 had a considerable influence on the adsorption of BTA.

3.2. The effect of main parameters on BTA removal by MMBC

The effects of various parameters (modifier types, biochar size, $ZnCl_2$ concentration, and aqueous solution pH) on BTA removal by prepared composite are presented in Figure 2(a)–2(d). The obtained results from the evaluation of several modifier efficiencies showed that $ZnCl_2$ had the highest performance in BC modifying for BTA adsorption. Chemical activation by $ZnCl_2$ presumably provides much more porous and higher surface area in activated carbons, thereby providing a high adsorption capacity. The reaction between carbon atoms and $ZnCl_2$ (dehydrating agent) promotes carbonaceous materials' decomposition in the extended carbon interlayers (Şahin *et al.* 2015). The use of $ZnCl_2$ in chemical activation improves the carbon content through the aromatic graphitic structure formation. The obtained results are consistent with findings in similar studies (Xia *et al.* 2016). As shown in Figure 2(b), MMBC particle size plays a vital role in BTA adsorption. As with decreasing the $ZnCl_2$-MBC size, the BTA removal increases, maximum BTA removal was attained at the size of <150 μm. Reducing adsorbent particle size increases specific surface area, followed by the surface energy and enhanced BTA removal efficiency. In addition, this trend is also related to the adsorbent surface area and the BTA diffusion rate. Generally, assuming that the adsorption rate depends only on the surface area (the surface area of the smaller particle is high); hence, the dispersion way is shortened in the small adsorbent particle, and it provides a better opportunity to make the adsorbed BTA penetrate all internal pore structure. Similar results have been reported previously (Liu *et al.* 2021).

In addition, increasing the $ZnCl_2$ concentration from 5 to 100 g/L produced BTA removal percentage growth from 76 to 94%, but it remained constant after increasing the concentration up to 200 g/L. This was possible because increase in $ZnCl_2$ concentration reaction may cause a part of the micro-pore structure to be destroyed due to the pores collapsing (Şahin *et al.* 2015). A similar study was conducted by Şahin *et al.* (2015). According to Figure 2(d), the highest BTA adsorption efficiency was obtained at neutral pH 7–8. pH played a significant role in the organics' adsorption from aqueous solutions because of the protonation/deprotonation of adsorbates and the alteration in the surface charge of adsorbents by pH changes (Sarker *et al.* 2017). BTA is a heterocyclic aromatic compound; therefore, π–π interactions between the aromatic ring of BTA and adsorbent might be possible. The hydrophobic and π–π interactions are not highly dependent on pH. The declined adsorption of BTA with increasing pH might be explained by a

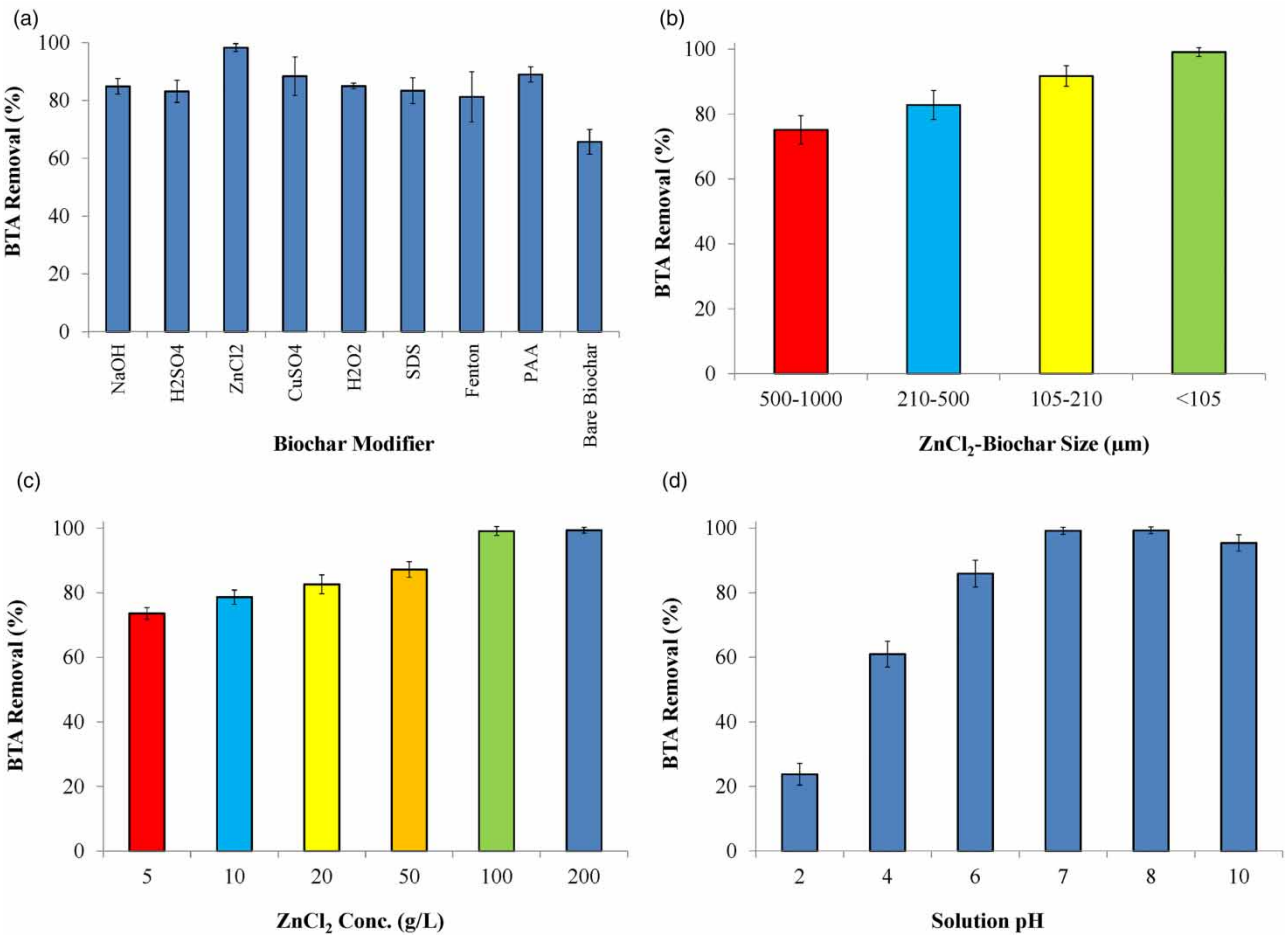

Figure 2 | The effect of (a) modifier types, (b) biochar size, (c) $ZnCl_2$ concentration and (d) pH on BTA removal by MMBC.

partial contribution of electro-static repulsions between the negative surface charge of adsorbent and the negative charge of the deprotonated BTA. Similarly, the decrease of q_t at an acidic pH might be because of repulsion between the positive adsorbent and positive or protonated BTA (Sarker *et al.* 2017).

3.3. RSM model analysis

The regression coefficients and the efficiency of BTA adsorption are described using the quadratic model as follows:

$$BTA\ Removal\ (\%) = 92.64 + 2.42X_T + 9.17X_D - 7.39X_{Co} - 1.51X_TX_D + 0.10X_TX_{Co} - 0.017X_DX_{Co} - 1.18X_T^2 - 5.14X_D^2 - 2.22X_{Co}^2 \quad (7)$$

Subjected to $-2 \leq X_i \leq +2$

The experimental and predicted values of BTA removal at various experimental conditions are illustrated in Table 4. The highest removal percentage was >99.9% in the 1st, 10th, 15th, 26th and 29th runs. Moreover, the results of ANOVA (Table 5) approved the ability of the employed model to design the optimization experiments. The relationship between predicted values of BTA adsorption efficiency against the experimental ones was also evaluated. Logically, since the coefficient of determination (R^2) is close to 1, the compatibility of the applied model is apparent. In addition, the high R^2 (0.987) confirms the robust correlation between the experimental and predicted data of BTA removal efficiency. It can be postulated that the model mentioned above could not predict only 1.13% of data. If the *F*-value of the model is more remarkable than tabulated *F* for a specific domain of degree of freedom, the proposed model is quite valid. As can be seen from Table 5, the *F*-value of the

model (298.51), which is the proportion of model mean square and residual error, is higher than the tabulated *F*-value that approves the statistical significance of the model. *F*-value for Lack of Fit was 22.08 (significant at <0.0001).

The normal probability plot of the data is shown in Figure 3(a). The apparent trend in the mentioned graph apparently has a normal distribution form which resembles a straight line. The plot of residuals versus predicted values (Figure 3(b)) revealed a randomized scattering trend in the adjacency of the centerline.

3.4. The influence of variables

The surface and contour plots as a promising method were drawn to illustrate BTA adsorption onto the MMBC surfaces at different chosen experimental variables. In Figure 4, the adsorption efficiency of BTA as a function of the combined effects of

Table 4 | Experimental design for the adsorption of BTA together with experimental and predicted response values

				BTA removal (%)		
Run number	Reaction time (min)	Adsorbent concentration (g/L)	Initial BTA concentration (mg/L)	Experimental	Predicted	Residual
1	50	0.8	30	99.5	101.5	1.98
2	35	0.55	50	92.6	92.6	0.04
3	50	0.3	70	72.9	71.6	1.28
4	50	0.3	30	85.7	86.1	0.45
5	5	0.55	50	83.0	83.1	0.07
6	35	1.05	50	92.1	90.4	1.69
7	50	0.8	70	85.3	86.9	1.56
8	65	0.55	50	93.5	92.7	0.75
9	35	1.05	50	92.5	90.4	2.09
10	35	0.55	10	99.9	98.5	1.36
11	35	0.55	50	92.4	92.6	0.24
12	20	0.3	30	79.3	78.5	0.84
13	50	0.3	70	71.8	71.6	0.21
14	20	0.8	30	98.1	99.9	1.77
15	50	0.8	30	99.3	101.5	2.18
16	35	0.55	50	93.0	92.6	0.36
17	20	0.3	30	78.5	78.5	0.04
18	5	0.55	50	81.9	83.1	1.17
19	20	0.3	70	64.7	63.5	1.20
20	35	0.55	90	68.7	69.0	0.29
21	20	0.8	70	85.2	84.8	0.36
22	35	0.05	50	52.1	53.7	1.61
23	65	0.55	50	94.0	92.7	1.25
24	20	0.3	70	65.7	63.5	2.20
25	20	0.8	70	84.2	84.8	0.64
26	35	0.55	10	99.8	98.5	1.26
27	50	0.8	70	86.8	86.9	0.06
28	35	0.55	50	93.3	92.6	0.66
29	20	0.8	30	99.4	99.9	0.47
30	35	0.05	50	52.3	53.7	1.41
31	50	0.3	30	86.1	86.1	0.02
32	35	0.55	90	67.4	69.0	1.57

Table 5 | ANOVA for the adequacy of the quadratic model

Source of variation	Sum of squares	Degree of freedom	Mean square	*F*-value	*p*-value
Model	5597.01	9	621.89	298.51	<0.0001
X_T	187.26	10	187.26	89.88	<0.0001
X_D	2693.61	1	2693.61	1292.93	<0.0001
X_{Co}	1749.55	1	1749.55	839.78	<0.0001
$X_T.X_D$	36.63	1	36.63	17.58	0.0004
$X_T.X_{Co}$	0.18	1	0.18	0.084	0.7743
$X_D.X_{Co}$	0.005	1	0.005	0.0023	0.9623
X_T^2	44.65	1	44.65	21.43	0.0001
X_D^2	846.66	1	846.66	406.40	<0.0001
X_{Co}^2	157.93	1	157.93	75.80	<0.0001
Residual	45.83	22	2.08		
Lack of Fit	39.72	5	7.94	22.08	<0.0001
Pure error	6.12	17	0.36		
Cor Total	5642.84	31			

$R^2 = 0.9919$, Adj $- R^2 = 0.9886$, C.V. % $= 1.72$, Predicted $- R^2 = 0.9821$, Adeq Precision $= 59.198$.
The 'Predicted $- R^2$' of 0.9821 is in reasonable agreement with the 'Adj $- R^2$' of 0.9886.

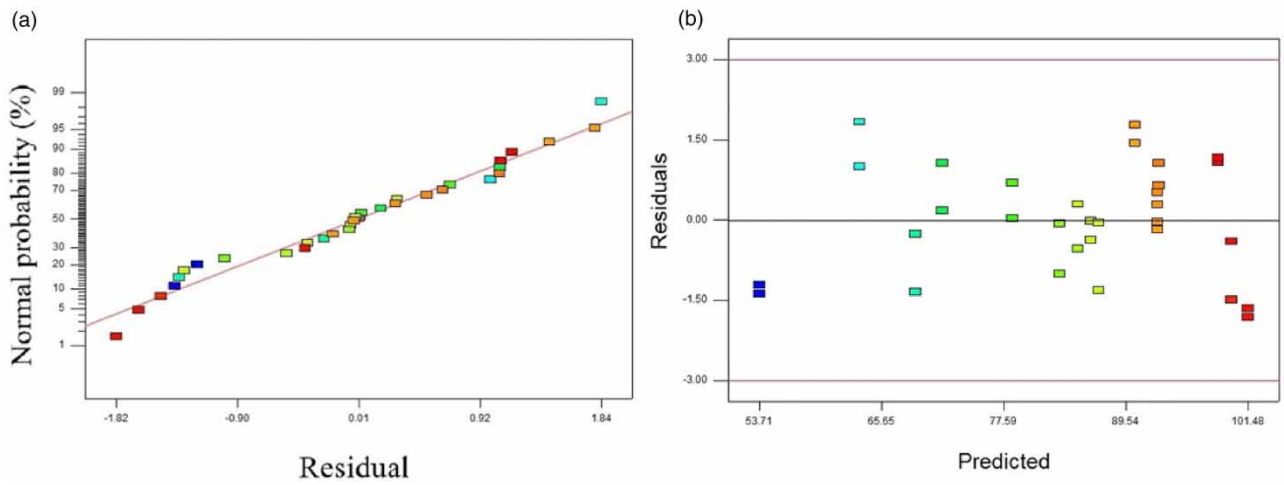

Figure 3 | (a) Normal probability plots for residual and (b) residuals versus predicted values.

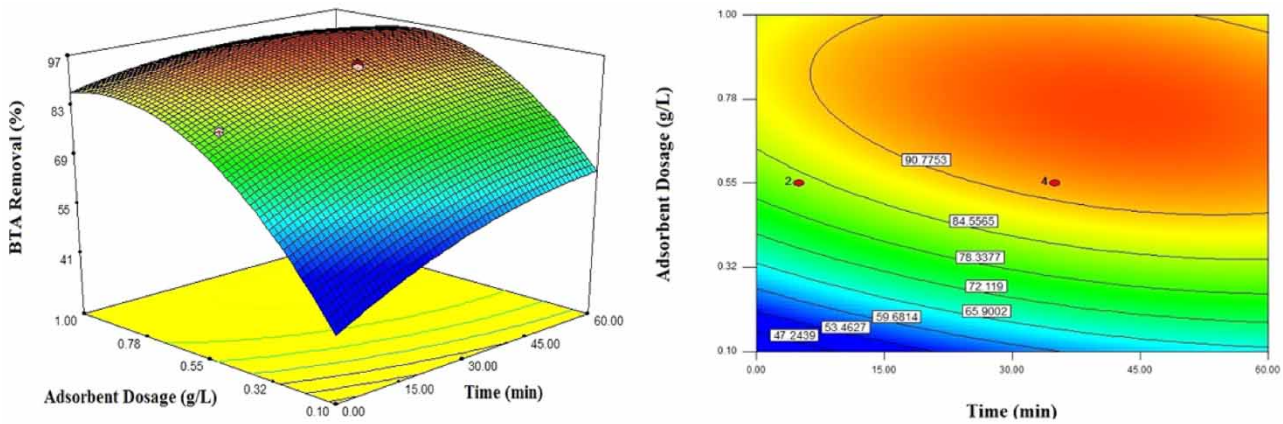

Figure 4 | The surface and contour plots of interaction effects of adsorbent dosage and reaction time on BTA removal efficiency.

adsorbent dosage and reaction time is shown. Based on Figure 4, an intensive increase in BTA adsorption occurred by increasing the reaction time from 2 to 60 min. It can be concluded that at the beginning of the experiment, due to the abundance of reactive sites, a large amount of BTA can be adsorbed, while the tendency of the adsorbent to sorb the adsorbate eventually declined due to saturation of the reactive sites. Additionally, the formation of insoluble silicates on the MMBC prevented the BTA from entering the internal sorption layer. The intraparticle diffusion in this phase may also be corresponding to a slower adsorption rate. A similar trend was observed previously in another work (Gwenzi *et al.* 2018; Zhu *et al.* 2020).

The interaction effects of reaction time and initial BTA concentration on the adsorption efficiency of BTA are depicted in Figure 5. According to Figure 5, at the constant MMBC concentration, increasing initial BTA concentration caused a significant decrease in the BTA adsorptive removal. The high concentration of BTA provides a thick layer of it onto the surfaces of modified biochar which certainly prevented BTA adsorption by the adsorbent (Srivastava *et al.* 2006). This trend can be explained by binding all BTA molecules with a composite surface at low concentration, while at high concentration, the available adsorption positions are reduced with build-up of BTA molecules on the surface of MMBC; this prevents the diffusion of more BTA molecules into the adsorbent pores. The low diffusion rate is related to pores, which are similar to the diffusing molecules. This phenomenon has previously been reported in the literature (Hameed *et al.* 2008).

The interaction effect of adsorbent dose and initial BTA concentration at a constant reaction time on BTA adsorption was also examined, and the results are given in Figure 6. By increasing the adsorbent dosage from 0.1 to 1 g/L, the adsorption efficiency increased from 35.5% to 94.4%. The most probable proof of our observation can be attributed to the increased effective specific surface area or exchangeable sites, followed by raising free active sites for adsorbate removal, which results in more interactions between BTA and adsorbent (Oliveira *et al.* 2008; Tan *et al.* 2015; Pourzamani *et al.* 2017; Dai *et al.* 2019).

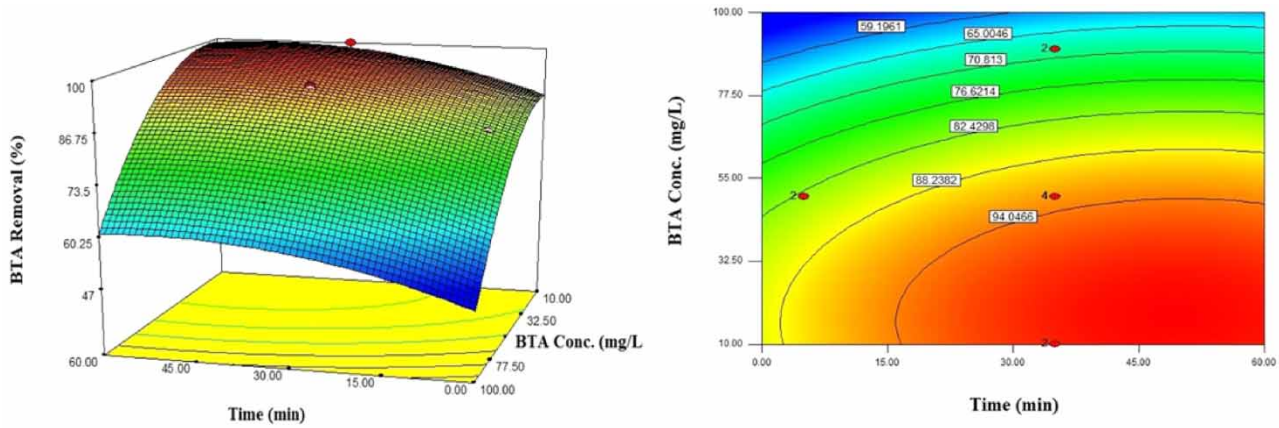

Figure 5 | The surface and contour plots of interaction effects of reaction time and initial BTA concentration on BTA removal efficiency.

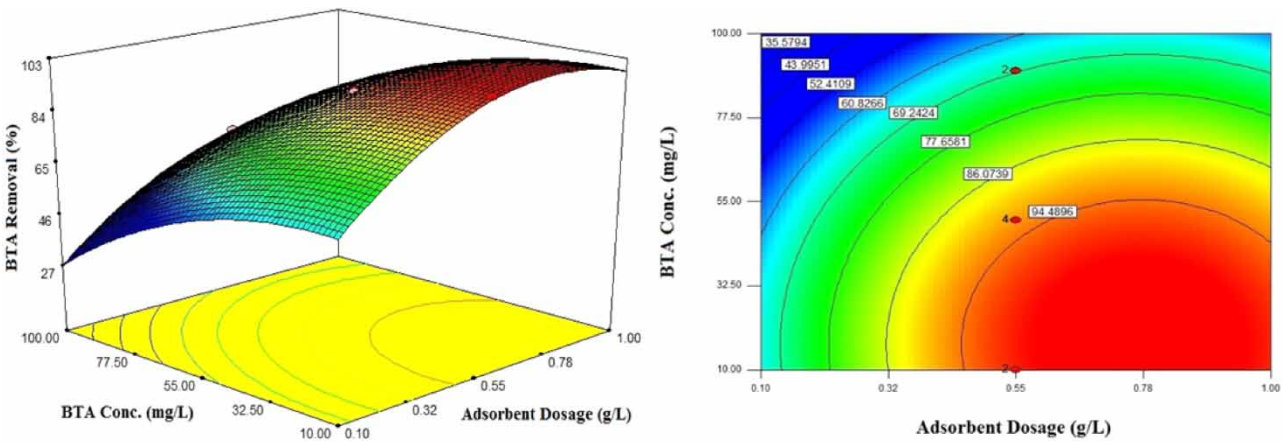

Figure 6 | The surface and contour plots of interaction effects of adsorbent dosage and initial BTA concentration on BTA removal efficiency.

3.5. Optimization of adsorption processes

For optimization of independent variables, the Derringer's desirability function method was utilized. In the mentioned method, the function scale operated between 0 and 1, in which 0 shows an entirely undesirable response and 1 represents a fully desired response (Haghighi *et al.* 2017).

The optimization results for BTA adsorption are given in Table 6. Accordingly, the optimum experimental conditions for removing BTA from aqueous solution were 35 min reaction time, 0.55 g/L adsorbent dose, and 50 mg/L initial BTA concentration. The predicted BTA adsorption efficiency was 92.6% at these optimal conditions, with an overall desirability value of 0.992. To further validate the model and to ensure that the model is representative of the actual system, six additional experiments were conducted under optimized conditions. Experimental responses were plotted versus the responses predicted by the model, and the results are illustrated in Figure 7. The predicted responses had correlations with the experimental ones with a high coefficient of determination of $R^2 = 0.992$ and $R^2 = 0.974$ for internal and external validation, respectively. It could be counted as undeniable proof of the suitability of the model.

3.6. Adsorption isotherm and kinetic studies

3.6.1. Isotherm studies

The adsorption isotherms are always considered feasible tools for determining the removal mechanism of pollutants in all adsorption systems. In order to obtain the isotherm parameters of BTA adsorption onto the MMBC, in general, the non-linear approach was adopted. The graphs of non-linear isotherms were prepared using MATLAB® 7.11.0 (R2015b). Five widely used isotherm models, namely Langmuir, Freundlich, Redlich–Peterson, Temkin, and Liu were applied. The results of non-linear isotherm studies of BTA adsorption at different temperatures (283 K, 298 K, and 313 K) are presented in Table 7. Accordingly, higher adsorption capacities of Langmuir isotherm (q_e) were observed at higher temperatures (q_m = 563.1 at 313 K, determination coefficient = 0.9799). Based on Table 7, at all studied temperatures, the Langmuir model, in comparison with the others, yielded the best fit with the experimental data of BTA adsorption with high coefficients of determination ($R^2 > 0.97$) using the non-linear approach. Such observation clearly indicates the homogeneous identity of BTA adsorption onto the monolayer surfaces of MMBC. The Langmuir isotherm is applied to explain single-solute systems, and

Table 6 | Optimum conditions selected for maximum possible BTA removal (%) by MMBC

Reaction time (min)	Adsorbent dosage (g/L)	Initial BTA concentration (mg/L)	Experimental %	Predicted %	Desirability
35	0.55	50	92.6	92.64	0.992

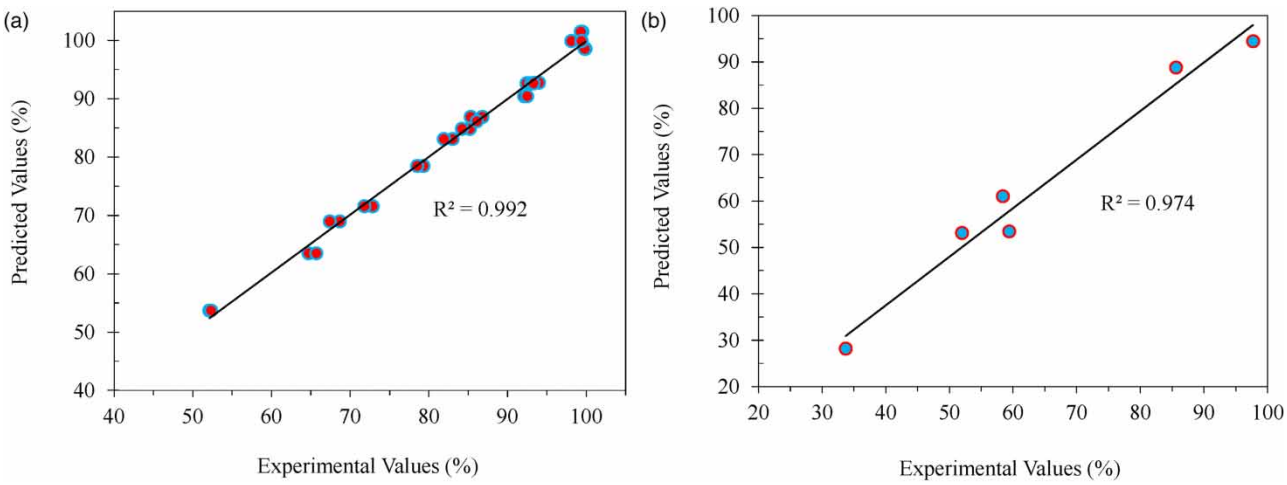

Figure 7 | The model validation graph (a) internal validation and (b) external validation.

Table 7 | Adsorption isotherms and their parameters

	Temperature		
Isotherm model	**283 K**	**298 K**	**313 K**
Langmuir	$K_L = 0.03717$ $q_m = 302.2$ SSE = 280.2 $R^2 = 0.9865$ $R^2adj = 0.9831$ RMSE = 8.369	$K_L = 0.09063$ $q_m = 462.9$ SSE = 746.9 $R^2 = 0.9916$ $R^2adj = 0.9895$ RMSE = 13.66	$K_L = 0.3017$ $q_m = 563.1$ SSE = 4044 $R^2 = 0.9799$ $R^2adj = 0.9749$ RMSE = 31.8
Freundlich	$K_F = 18.24$ $n = 1.591$ SSE = 776.1 $R^2 = 0.9626$ $R^2adj = 0.9533$ RMSE = 13.93	$K_F = 60.28$ $n = 1.95$ SSE = 1555 $R^2 = 0.9825$ $R^2adj = 0.9782$ RMSE = 19.71	$K_F = 147.8$ $n = 2.495$ SSE = 1318 $R^2 = 0.9935$ $R^2adj = 0.9918$ RMSE = 18.15
Redlich–Peterson	$K_{RP} = 11.23$ $a_{RP} = 0.03716$ g = 1 SSE = 280.2 $R^2 = 0.9865$ $R^2adj = 0.9831$ RMSE = 8.369	$K_{RP} = 41.95$ $a_{RP} = 0.09063$ g = 1 SSE = 746.9 $R^2 = 0.9916$ $R^2adj = 0.986$ RMSE = 15.78	$K_{RP} = 824.7$ $a_{RP} = 13.37$ g = 0.6291 SSE = 971 $R^2 = 0.9952$ $R^2adj = 0.992$ RMSE = 17.99
Liu	$K_a = 0.03716$ $n = 1$ $q_m = 302.2$ SSE = 280.2 $R^2 = 0.9865$ $R^2adj = 0.9831$ RMSE = 8.369	$K_a = 0.05947$ $n = 0.8491$ $q_m = 547.7$ SSE = 635.8 $R^2 = 0.9929$ $R^2adj = 0.9881$ RMSE = 14.56	$K_a = 0.03512$ n = 0.5509 $q_m = 1085$ SSE = 458.1 $R^2 = 0.9977$ $R^2adj = 0.9962$ RMSE = 12.36
Temkin	$A_T = 0.3872$ B = 65.24 SSE = 2.916 $R^2 = 0.9999$ $R^2adj = 0.9998$ RMSE = 0.8538	$A_T = 2.357$ B = 73.27 SSE = 6020 $R^2 = 0.9323$ $R^2adj = 0.9154$ RMSE = 38.79	$A_T = 18.81$ B = 74.63 SSE = 1.587e + 04 $R^2 = 0.9212$ $R^2adj = 0.9015$ RMSE = 62.99

it is assumed that there are particular homogenous sites in the adsorbent and no significant interaction exists between diverse types of adsorbed substances. On the other hand, the Freundlich isotherm is used to explain heterogeneous systems (Suganya 2019). The adsorption capacities of BTA removal using various adsorbents are reported in Table 8, which confirms the high capability of $ZnCl_2$-activated magnetic biochar in eliminating BTA from aqueous solutions.

3.6.2. Kinetic studies

Kinetics describes solute uptake rates and defines the residence time of the adsorbate at the solid-liquid interface. Additionally, valuable insights into the reaction pathways and the adsorption mechanisms can be achieved via kinetic studies. Kinetic experiments were performed using the MMBC dosage, solution pH, and the initial BTA concentration of 1.0 g L^{-1}, 7.0, and 100 mg L^{-1}, respectively, at 283 K, 298 K, and 313 K (Figure 8).

As shown in Figure 8, BTA uptake seems to have occurred in two steps. The first step involved swift uptake within the first 10 min of the contact followed by the subsequent removal of BTA, which continued for a relatively short period until adsorption equilibrium was obtained. The kinetic parameters acquired from non-linear fitting results are presented in Table 9. Based on the higher values of the adjusted determination coefficient ($R^2adj > 0.99$) and the lower values of SSE and the RMSE, it can be concluded that the kinetic models of the Avrami fractional-order kinetic model were the most appropriate for representing BTA adsorption onto MMBC.

Table 8 | Comparison of the adsorption capacities of applied adsorbents with the other adsorbents for BTA removal from aqueous solutions

Adsorbent	Adsorption capacity (mg g^{-1})	Reference
Soil	0.073 – 0.195	Pourzamani *et al.* (2017)
Zn–Al–O binary metal oxide	9.51	Tan *et al.* (2015)
Zn–Al LDO	1910.0	Haghighi *et al.* (2017)
ZIF–67/MG[a]	257.9	Kim & Kim (2019)
ZIF–8(Zn)[b]	260	Khan *et al.* (2020)
ZIF–67 (Co)[c]	270	Khan *et al.* (2020)
MAF–5 (Co)[d]	389	Khan *et al.* (2020)
Zeolitic imidazolate framework–8 (ZIF–8)	298.5	Zaheer *et al.* (2019)
MMBC	462.9	This study

[a]Zeolitic imidazolate framework–67/magnetic reduced graphene oxide.
[b]Zeolitic imidazolate Zn framework–8.
[c]Zeolitic imidazolate Co framework–67.
[d]Co-based metal azolate framework.

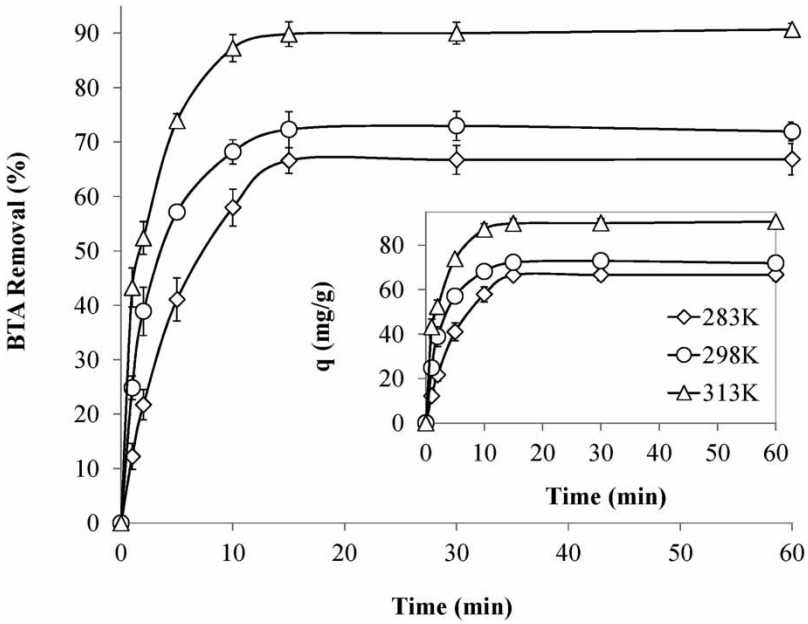

Figure 8 | Effect of contact time on BTA adsorption onto MMBC (adsorbent dose: 1.0 g L^{-1}, pH: 7.0, BTA: 100 mg L^{-1}).

3.7. Thermodynamic studies

Temperature is an essential parameter that governs the adsorption process. Thermodynamic studies were performed at different temperatures (283, 298, and 313 K) to calculate the thermodynamic parameters of the BTA adsorption process. The thermodynamic parameters of Arrhenius activation energy (Ea) and change in free energy (ΔG°), enthalpy (ΔH°), and entropy (ΔS°) of the adsorption process were calculated according to Equations (8)–(10) (Kim & Kim 2019). More details of these parameters are given in the Supplementary material (available with the online version of this paper):

$$\ln k_{AV} = \ln k_o - \frac{Ea}{RT} \tag{8}$$

$$\Delta G^o = -RT \ln K_L \tag{9}$$

$$\ln K_L = \frac{\Delta S^o}{R} - \frac{\Delta H^o}{RT} \tag{10}$$

Table 9 | Adsorption rate constants for five kinetic models of BTA adsorption on MMBC

	Temperature		
Kinetic	**283 K**	**298 K**	**313 K**
Pseudo-first-order (Lagergern)	$k_f = 0.1944$ $q_e = 67.73$ SSE = 9.045 $R^2 = 0.9982$ R^2adj = 0.998 RMSE = 1.228	$k_f = 0.3741$ $q_e = 71.5$ SSE = 25.16 $R^2 = 0.9951$ R^2adj = 0.9943 RMSE = 2.048	$k_f = 0.4955$ $q_e = 88.36$ SSE = 146.4 $R^2 = 0.98$ R^2adj = 0.9767 RMSE = 4.939
Pseudo-second-order (Ho)	$k_S = 0.003169$ $q_e = 76.74$ SSE = 99.19 $R^2 = 0.9807$ R^2adj = 0.9775 RMSE = 4.066	$k_S = 0.006624$ $q_e = 78.23$ SSE = 35.82 $R^2 = 0.993$ R^2adj = 0.9919 RMSE = 2.443	$k_S = 0.007719$ $q_e = 95.2$ SSE = 53.38 $R^2 = 0.9927$ R^2adj = 0.9915 RMSE = 2.983
Avrami fractional order	$k_{AV} = 0.1962$ $n_{AV} = 1.031$ $q_e = 67.52$ SSE = 8.3 $R^2 = 0.9984$ R^2adj = 0.9977 RMSE = 1.288	$k_{AV} = 0.3494$ $n_{AV} = 0.8183$ $q_e = 72.8$ SSE = 2.743 $R^2 = 0.9995$ R^2adj = 0.9993 RMSE = 0.7406	$k_{AV} = 0.4473$ $n_{AV} = 0.658$ $q_e = 91.43$ SSE = 23.49 $R^2 = 0.9968$ R^2adj = 0.9955 RMSE = 2.167
Elovich	$\alpha = 37.53$ $\beta = 0.06476$ SSE = 362.1 $R^2 = 0.9297$ R^2adj = 0.918 RMSE = 7.769	$\alpha = 170.6$ $\beta = 0.08219$ SSE = 313.9 $R^2 = 0.9389$ R^2adj = 0.9288 RMSE = 7.232	$\alpha = 579.$ $\beta = 0.07887$ SSE = 318 $R^2 = 0.9566$ R^2adj = 0.9494 RMSE = 7.28
Intraparticle diffusion	C = 12.74 $k_{id} = 9.284$ SSE = 1233 $R^2 = 0.7606$ R^2adj = 0.7207 RMSE = 14.33	C = 23.71 $k_{id} = 8.696$ SSE = 1703 $R^2 = 0.6686$ R^2adj = 0.6134 RMSE = 16.85	C = 34.41 $k_{id} = 10.12$ SSE = 2672 $R^2 = 0.6352$ R^2adj = 0.5744 RMSE = 21.1

The magnitude of activation energy gives information about the type of adsorption. The physisorption process usually has energies in the range of 5–40 kJ/mol, while higher activation energies (40–800 kJ/mol) suggest chemisorption (Zaheer *et al.* 2019). The activation energy was calculated to be 20.3 kJ/mol, indicating that the adsorption of BTA onto the MMBC was a physisorption process (<40 kJ/mol) (Kim & Kim 2019; Pourzamani *et al.* 2017). According to the thermodynamic results, the obtained $\Delta G°$ was negative at all temperatures, indicating that the process is spontaneous and more favorable at high temperatures (see Table 10). The positive value of $\Delta H°$ (55.2 kJ/mol) also showed that the process of BTA adsorption onto MMBC is endothermic. The enthalpy change value between 2.1 and 20.9 kJ/mol is frequently considered to indicate physical adsorption processes, whereas, for chemical adsorption, it lies in the range of 80–200 kJ/mol. In this study, the $\Delta H°$ value was 55.2 kJ/mol, suggesting that the transportation of BTA from the aqueous solution to the MMBC surface occurred physically, which is consistent with the results obtained from the activation energy of the adsorption (Kim & Kim 2019). Additionally,

Table 10 | The values of thermodynamic parameters of BTA adsorption on MMBC

T (K)	$\Delta H°$ (kJ/mol)	$\Delta S°$ (J/mol)	$\Delta G°$ (kJ/mol)
283	55.2	275	–22.7
298			–26.5
313			–30.9

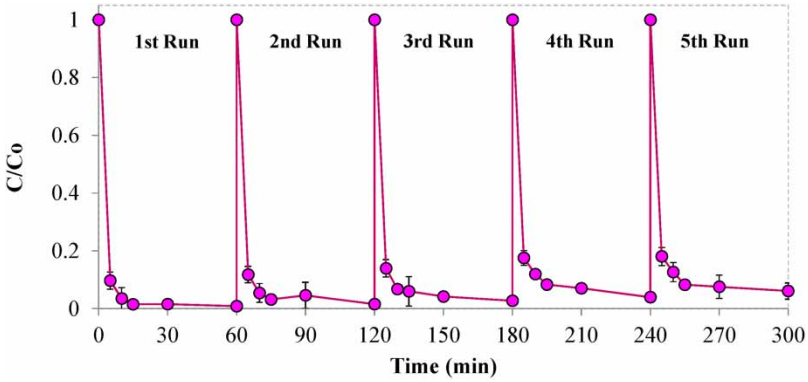

Figure 9 | Examining the adsorptive removal of BTA at five consecutive cycles using MMBC.

from the positive value of $\Delta S°$, it can be concluded that an increase occurred in the randomness of the solid/surface interface at the internal structure of the BTA adsorption onto the applied composite.

3.8. Reusability of MMBC

The reusability of the adsorbents is an essential criterion for their commercial applications. Simple methanol washing was performed to recover MMBC for reuse in other adsorption cycles since BTA is readily soluble in methanol. As represented in Figure 9, the adsorption percentage of BTA by MMBC decreased non-significantly from 99.2 to 93.9% after the fifth cycle. This proves that the synthesized MMBC can be recycled and reused for at least five successive cycles with an adsorption efficiency of >90%. It was also observed that desorption efficiencies did not noticeably change by increasing desorption cycles. More than 93.5% of the adsorbed BTA could be desorbed and recovered from the MMBC surface in the presence of methanol in the fifth cycle. These results suggest that the MMBC has a good potential for regeneration and reusability. Therefore, it can serve as a cost-effective and robust adsorbent for BTA removal from aqueous solutions in industrial applications based on simple and easy renewal with solvent treatment.

4. CONCLUSION

In the present research, the MMBC composite was synthesized and characterized by various techniques for BTA adsorption from aqueous solutions. Therefore, CCD was applied to investigate and optimize BTA adsorption variables such as BTA initial concentration, pH value, reaction time, and composite dosage. Based on the obtained results, the following conclusions are reached:

- SEM and EDX analysis announced that $ZnCl_2$ successfully modified Fe_3O_4 particles uniformly distributed on BC and prepared composed.
- Among various chemicals, $ZnCl_2$ was the best modifier for modification of MBC, and $ZnCl_2$/MBC had the highest performance in BTA adsorption.
- The primary operational parameter evaluation indicated that the BTA removal rate increases with increasing MMBC dosage and reaction time, while it declines with increasing initial BTA concentration.
- According to Derringer's desirability function method, the optimum condition was found to be 35 min reaction time, 0.55 g/L adsorbent dose, and 50 mg/L initial BTA concentration.
- The kinetic studies illustrated that the Avrami fractional-order model could describe BTA adsorption behavior well. Also, the adsorption isotherm was fitted with a non-linear Langmuir model with a maximum adsorption capacity of 563.1 mg/g. Moreover, thermodynamic parameters indicated a feasible, spontaneous, and endothermic physisorption.
- The regeneration assessments approved that the MMBC composite had appealing features for field application.

ACKNOWLEDGEMENTS

The authors would like to thank the Research and Technology Deputy of Ahvaz Jundishapur University of Medical Sciences for financial support (grant no: ETRC-9505).

DATA AVAILABILITY STATEMENT

All relevant data are included in the paper or its Supplementary Information.

REFERENCES

Abdessalem, A. K., Oturan, N., Bellakhal, N., Dachraoui, M. & Oturan, M. A. 2008 Experimental design methodology applied to electro-Fenton treatment for degradation of herbicide chlortoluron. *Applied Catalysis B: Environmental* **78**, 334–341.

Bernal-Martínez, L. A., Barrera-Díaz, C., Natividad, R. & Rodrigo, M. A. 2013 Effect of the continuous and pulse in situ iron addition onto the performance of an integrated electrochemical–ozone reactor for wastewater treatment. *Fuel* **110**, 133–140.

Bonvin, F., Jost, L., Randin, L., Bonvin, E. & Kohn, T. 2016 Super-fine powdered activated carbon (SPAC) for efficient removal of micropollutants from wastewater treatment plant effluent. *Water Research* **90**, 90–99.

Cui, L., Noerpel, M. R., Scheckel, K. G. & Ippolito, J. A. 2019 Wheat straw biochar reduces environmental cadmium bioavailability. *Environment International* **126**, 69–75.

Dai, Y., Zhang, N., Xing, C., Cui, Q. & Sun, Q. 2019 The adsorption, regeneration and engineering applications of biochar for removal organic pollutants: a review. *Chemosphere* **223**, 12–27.

Ding, Y., Yang, C., Zhu, L. & Zhang, J. 2010 Photoelectrochemical activity of liquid phase deposited TiO_2 film for degradation of benzotriazole. *Journal of Hazardous Materials* **175**, 96–103.

Giger, W., Schaffner, C. & Kohler, H. P. E. 2006 Benzotriazole and tolyltriazole as aquatic contaminants. 1. Input and occurrence in rivers and lakes. *Environmental Science & Technology* **40**, 7186–7192.

Gokulan, R., Ganesh Prabhu, G. & Jegan, J. 2019 A novel sorbent ulva lactuca-derived biochar for remediation of Remazol Brilliant Orange 3R in packed column. *Water Environment Research* **91**, 642–649.

Grillo, F., Tee, D. W., Francis, S. M., Früchtl, H. & Richardson, N. V. 2013 Initial stages of benzotriazole adsorption on the Cu (111) surface. *Nanoscale* **5**, 5269–5273.

Gwenzi, W., Nyambishi, T. J., Chaukura, N. & Mapope, N. 2018 Synthesis and nutrient release patterns of a biochar-based N–P–K slow-release fertilizer. *International Journal of Environmental Science and Technology* **15**, 405–414.

Haghighi, M., Rahmani, F., Dehghani, R., Tehrani, A. M. & Miranzadeh, M. B. 2017 Photocatalytic reduction of Cr (VI) in aqueous solution over ZnO/HZSM-5 nanocomposite: optimization of ZnO loading and process conditions. *Desalin Water Treat* **58**, 168–180.

Haghighi, M., Rahmani, F., Kariminejad, F. & Sene, R. A. 2019 Photodegradation of lignin from pulp and paper mill effluent using TiO_2/PS composite under UV-LED radiation: optimization, toxicity assessment and reusability study. *Process Safety and Environmental Protection* **122**, 48–57.

Hameed, B. H., Tan, I. A. W. & Ahmad, A. L. 2008 Optimization of basic dye removal by oil palm fibre-based activated carbon using response surface methodology. *Journal of Hazardous Materials* **158**, 324–332.

Harris, C. A., Routledge, E. J., Schaffner, C., Brian, J. V., Giger, W. & Sumpter, J. P. 2007 Benzotriazole is antiestrogenic in vitro but not in vivo. *Environmental Toxicology and Chemistry: An International Journal* **26**, 2367–2372.

Janna, H., Scrimshaw, M. D., Williams, R. J., Churchley, J. & Sumpter, J. P. 2011 From dishwasher to tap? Xenobiotic substances benzotriazole and tolyltriazole in the environment. *Environmental Science & Technology* **45**, 3858–3864.

Jeon, C. 2019 Removal of Cr (VI) from aqueous solution using amine-impregnated crab shells in the batch process. *Journal of Industrial and Engineering Chemistry* **77**, 111–117.

Khan, Z. H., Gao, M., Qiu, W., Islam, M. S. & Song, Z. 2020 Mechanisms for cadmium adsorption by magnetic biochar composites in an aqueous solution. *Chemosphere* **246**, 125701.

Kim, Y. S. & Kim, J. H. 2019 Isotherm, kinetic and thermodynamic studies on the adsorption of paclitaxel onto Sylopute. *The Journal of Chemical Thermodynamics* **130**, 104–113.

Li, J., Lu, X., Ou, J. & Cheng, J. 2012 Adsorption mechanism of benzotriazole on copper surface in CMP based slurries containing peroxide and glycine. In: *ICPT 2012-International Conference on Planarization/CMP Technology*. 2012, pp. 1–6.

Liu, Q., Jiang, S., Su, X., Zhang, X., Cao, W. & Xu, Y. 2021 Role of the biochar modified with $ZnCl_2$ and $FeCl_3$ on the electrochemical degradation of nitrobenzene. *Chemosphere* **275**, 129966.

Liu, S., Li, J., Xu, S., Wang, M., Zhang, Y. & Xue, X. 2019 A modified method for enhancing adsorption capability of banana pseudostem biochar towards methylene blue at low temperature. *Bioresource Technology* **282**, 48–55.

Mawhinney, D. B., Vanderford, B. J. & Snyder, S. A. 2012 Transformation of 1 H-benzotriazole by ozone in aqueous solution. *Environmental Science & Technology* **46**, 7102–7111.

Mezzi, A., Angelini, E., De Caro, T., Grassini, S., Faraldi, F., Riccucci, C. & Ingo, G. M. 2012 Investigation of the benzotriazole inhibition mechanism of bronze disease. *Surface and Interface Analysis* **44**, 968–971.

Najafpoor, A. A., Sani, O. N., Alidadi, H., Yazdani, M., Fezabady, A. A. N. & Taghavi, M. 2019 Optimization of ciprofloxacin adsorption from synthetic wastewaters using γ-Al_2O_3 nanoparticles: an experimental design based on response surface methodology. *Colloid and Interface Science Communications* **33**, 100212.

Oliveira, L. S., Franca, A. S., Alves, T. M. & Rocha, S. D. 2008 Evaluation of untreated coffee husks as potential biosorbents for treatment of dye contaminated waters. *Journal of Hazardous Materials* **155**, 507–512.

Pourzamani, H., Parastar, S. & Hashemi, M. 2017 The elimination of xylene from aqueous solutions using single wall carbon nanotube and magnetic nanoparticle hybrid adsorbent. *Process Safety and Environmental Protection* **109**, 688–696.

Pritchard, J. C., Cho, Y. M., Ashoori, N., Wolfand, J. M., Sutton, J. D., Carolan, M. E., Gamez, E., Doan, K., Wiley, J. S. & Luthy, R. G. 2018 Benzotriazole uptake and removal in vegetated biofilter mesocosms planted with Carex praegracilis. *Water* **10**, 1605.

Rangabhashiyam, S., Anu, N., Nandagopal, M. G. & Selvaraju, N. 2014 Relevance of isotherm models in biosorption of pollutants by agricultural byproducts. *Journal of Environmental Chemical Engineering* **2**, 398–414.

Rezakazemi, M. & Shirazian, S. 2019 Lignin-chitosan blend for methylene blue removal: adsorption modeling. *Journal of Molecular Liquids* **274**, 778–791.

Rhodes-Dicker, L. & Passeport, E. 2019 Effects of cold-climate environmental factors temperature and salinity on benzotriazole adsorption and desorption in bioretention cells. *Ecological Engineering* **127**, 58–65.

Richardson, S. D. & Ternes, T. A. 2018 Water analysis: emerging contaminants and current issues. *Anal Chem* **90**, 398–428.

Şahin, Ö., Saka, C., Ceyhan, A. A. & Baytar, O. 2015 Preparation of high surface area activated carbon from Elaeagnus angustifolia seeds by chemical activation with zncl2 in one-step treatment and its iodine adsorption. *Separation Science and Technology* **50**, 886–891.

Sarangi, B., Jana, U., Sahoo, J., Mohanta, G. P. & Manna, P. K. 2018 Systematic approach for the formulation and optimization of atorvastatin loaded solid lipid NANOAPARTICLES using response surface methodology. *Biomedical Microdevices* **20**, 1–12.

Sarker, M., Bhadra, B. N., Seo, P. W. & Jhung, S. H. 2017 Adsorption of benzotriazole and benzimidazole from water over a Co-based metal azolate framework MAF-5 (Co). *Journal of Hazardous Materials* **324**, 131–138.

Srivastava, V. C., Swamy, M. M., Mall, I. D., Prasad, B. & Mishra, I. M. 2006 Adsorptive removal of phenol by bagasse fly ash and activated carbon: equilibrium, kinetics and thermodynamics. *Colloids and Surfaces A: Physicochemical and Engineering Aspects* **272**, 89–104.

Suganya, S. 2019 An investigation of adsorption parameters on ZVI-AC nanocomposite in the displacement of Se (IV) ions through CCD analysis. *Journal of Industrial and Engineering Chemistry* **75**, 211–223.

Syafiuddin, A., Salmiati, S., Hadibarata, T., Salim, M. R., Kueh, A. B. H. & Suhartono, S. 2019 Removal of silver nanoparticles from water environment: experimental, mathematical formulation, and cost analysis. *Water, Air, & Soil Pollution* **230**, 1–15.

Tan, X., Liu, Y., Zeng, G., Wang, X., Hu, X., Gu, Y. & Yang, Z. 2015 Application of biochar for the removal of pollutants from aqueous solutions. *Chemosphere* **125**, 70–85.

Vilardi, G., Di Palma, L. & Verdone, N. 2018 Heavy metals adsorption by banana peels micro-powder: equilibrium modeling by non-linear models. *Chinese Journal of Chemical Engineering* **26**, 455–464.

Wang, X., Zhuo, N., Fu, C., Tian, Z., Li, H., Zhang, J., Wu, W., Yang, Z. & Yang, W. 2017 Enhanced selective adsorption of benzotriazole onto nanosized zeolitic imidazolate frameworks confined in polystyrene anion exchanger. *Chemical Engineering Journal* **328**, 816–824.

Weiss, S. & Reemtsma, T. 2008 Membrane bioreactors for municipal wastewater treatment–a viable option to reduce the amount of polar pollutants discharged into surface waters? *Water Research* **42**, 3837–3847.

Xia, D., Tan, F., Zhang, C., Jiang, X., Chen, Z., Li, H., Zheng, Y., Li, Q. & Wang, Y. 2016 $ZnCl_2$-activated biochar from biogas residue facilitates aqueous As (III) removal. *Applied Surface Science* **377**, 361–369.

Xu, B., Qi, F., Wu, F., Xu, Q. & Chen, Z. 2014 Adsorption kinetics of benzotriazole and its derivatives by nano Zn–Al–O. *Journal of Nanoscience and Nanotechnology* **14**, 7272–7278.

Yan, L., Liu, Y., Zhang, Y., Liu, S., Wang, C., Chen, W., Liu, C., Chen, Z. & Zhang, Y. 2020 ZnCl2 modified biochar derived from aerobic granular sludge for developed microporosity and enhanced adsorption to tetracycline. *Bioresource Technology* **297**, 122381.

Yin, Q., Ren, H., Wang, R. & Zhao, Z. 2018 Evaluation of nitrate and phosphate adsorption on Al-modified biochar: influence of Al content. *Science of the Total Environment* **631**, 895–903.

Zaheer, Z., Bawazir, W. A., Al-Bukhari, S. M. & Basaleh, A. S. 2019 Adsorption, equilibrium isotherm, and thermodynamic studies to the removal of acid orange 7. *Materials Chemistry and Physics* **232**, 109–120.

Zhang, S., Abdalla, M. A., Luo, Z. & Xia, S. 2018 The wheat straw biochar research on the adsorption/desorption behaviour of mercury in wastewater. *Desalin Water Treat* **112**, 147–160.

Zhou, Y., He, Y., He, Y., Liu, X., Xu, B., Yu, J., Dai, C., Huang, A., Pang, Y. & Luo, L. 2019 Analyses of tetracycline adsorption on alkali-acid modified magnetic biochar: site energy distribution consideration. *Science of the Total Environment* **650**, 2260–2266.

Zhu, L., Zhao, N., Tong, L., Lv, Y. & Li, G. 2018 Characterization and evaluation of surface modified materials based on porous biochar and its adsorption properties for 2, 4-dichlorophenoxyacetic acid. *Chemosphere* **210**, 734–744.

Zhu, D., Chen, Y., Yang, H., Wang, S., Wang, X., Zhang, S. & Chen, H. 2020 Synthesis and characterization of magnesium oxide nanoparticle-containing biochar composites for efficient phosphorus removal from aqueous solution. *Chemosphere* **247**, 125847.

First received 14 September 2021; accepted in revised form 1 March 2022. Available online 16 March 2022